Photoelectron Spectra and Ion Chemistry of Imidazolide†

Adam J. Gianola, Takatoshi Ichino, Rebecca L. Hoenigman, Shuji Kato, Veronica M. Bierbaum,* and W. Carl Lineberger*

JILA, University of Colorado and National Institute of Standards and Technology, and Department of Chemistry and Biochemistry, University of Colorado, Boulder, Colorado 80309-0440

Received: June 29, 2005; In Final Form: August 17, 2005

The 351.1 nm photoelectron spectrum of imidazolide anion has been measured. The electron affinity (EA) of the imidazolyl radical is determined to be 2.613 ± 0.006 eV. Vibrational frequencies of 955 ± 15 and 1365 ± 20 cm^{-1} are observed in the spectrum of the $^2B_1$ ground state of the imidazolyl radical. The main features in the spectrum are well-reproduced by Franck−Condon simulation based on the optimized geometries and the normal modes obtained at the B3LYP/6-311++G(d,p) level of density functional theory. The two vibrational frequencies are assigned to totally symmetric modes with C−C and N−C stretching motions. Overtone peaks of an in-plane nontotally symmetric mode are observed in the spectrum and attributed to Fermi resonance. Also observed is the photoelectron spectrum of the anion formed by deprotonation of imidazole at the C5 position. The EA of the corresponding radical, 5-imidazolyl, is 1.992 ± 0.010 eV. The gas phase acidity of imidazole has been determined using a flowing afterglow-selected ion tube; $\Delta_{acid}G_{298} = 342.6 \pm 0.4$ and $\Delta_{acid}H_{298} = 349.7 \pm 0.5$ kcal mol^{-1}. From the EA of imidazolyl radical and gas phase acidity of imidazole, the bond dissociation energy for the N−H bond in imidazole is determined to be 95.1 ± 0.5 kcal mol^{-1}. These thermodynamic parameters for imidazole and imidazolyl radical are compared with those for pyrrole and pyrrolyl radical, and the effects of the additional N atom in the five-membered ring are discussed.

Introduction

Recent interest in a homonuclear polynitrogen compound, pentazolide (N_5^-),[1−7] as a high energy density material has prompted us to initiate a systematic investigation of the properties of its isoelectronic species: five-membered carbon−nitrogen heterocyclic compounds. Previously, we reported a photoelectron spectroscopic study of pyrrolide anion, which contains one N atom in the five-membered ring.[8] The electron affinity (EA) of pyrrolyl radical was experimentally determined, and combined with the N−H bond dissociation energy (BDE) of pyrrole in a thermochemical cycle, the gas phase acidity of pyrrole was accurately derived. The vibrational structure and potential energy surface of the electronic ground state of pyrrolyl were also studied. Continuing this investigation, we explore five-membered heterocyclic compounds containing two N atoms. Depending on the arrangement of the two N atoms in the ring, two isomers are possible, imidazole and pyrazole. The two N atoms are not directly bonded to each other in imidazole, while they are adjacent in pyrazole. In this paper, we discuss imidazole, and our studies on pyrazole will be reported in forthcoming papers.[9,10]

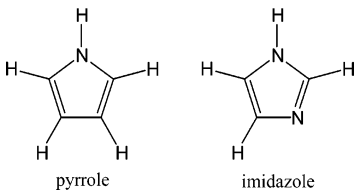

The imidazole ring is found in the side chain of the amino acid, histidine. The interaction of the histidine residue with other components in biological systems (e.g., protein residues, metal centers, etc.) influences or governs protein conformations and, therefore, their properties. Thus, histidine has often been the focus of attention in studies of enzyme structures.

Histidine can be compared with tyrosine, which contains phenol. Tyrosine has been extensively studied because of its active role in many enzymatic reactions; e.g., oxidation of H_2O to O_2 in photosystem II,[11,12] reduction of O_2 to H_2O in cytochrome *c* oxidase,[13,14] conversion of nucleotide to deoxynucleotide in ribonucleotide reductase,[15] etc. An oxidized form of tyrosine, tyrosyl radical (*para*-substituted phenoxyl radical), is a key intermediate in these redox processes, and many spectroscopic studies can be found in the literature for tyrosyl radical as well as for phenoxyl radical, e.g., ESR,[16,17] IR,[18] resonance Raman,[19−22] photoelectron spectroscopy,[23] etc.

On the other hand, there have been few reports on histidinyl radical in biological systems. Its relatively high reduction potential[24] may prevent its direct involvement in redox processes. However, a few systems have recently been reported where oxidation of histidine may be important. For instance, cross-linkage between tyrosine and histidine has been found in the active site of cytochrome *c* oxidases.[25−29] In studies on covalently linked phenol-imidazole model compounds,[30−32] it has been found that there is appreciable electronic interaction between the two components in the radical form, which renders it some imidazolyl character. Another system is Cu,Zn-superoxide dismutase (SOD). This enzyme has been the focus of intense investigation with respect to a fatal motor neuron disease, familial amyotrophic lateral sclerosis (ALS).[33,34] A consensus has been emerging that SOD aggregation has a causal relation to the toxicity of the disease.[34−36] However, the aggregation

† Part of the special issue "Jack Simons Festschrift".

* To whom correspondence should be addressed. (V.M.B.) E-mail: veronica.bierbaum@colorado.edu. (W.C.L.) E-mail: wcl@jila.colorado.edu.

10.1021/jp053566o CCC: $30.25
Published on Web 09/24/2005

mechanism is still under serious debate. Aberrant chemistry has been studied in relation to the aggregation of the enzyme.[37,38] A possible pathway to the aggregation has been proposed, which involves oxidation of histidine.[39,40] Histidinyl radical itself has been detected by spin-trap electron spin resonance (ESR) measurements when SOD is treated with H_2O_2 or peroxynitrite.[41,42]

Information on the properties of the imidazolyl radical will be useful in understanding these biological processes. ESR spectra of imidazolyl have been reported, which elucidate the unpaired electron spin density of the electronic ground state of the radical.[43] However, the vibrational structure of imidazolyl has not been reported.[44] We have measured the photoelectron spectrum of imidazolide anion, presented in this paper, which reflects the transition between the anion ground state and the imidazolyl ground state. Certain vibrational modes of imidazolyl appear in the spectrum, following the Franck−Condon principle. This paper represents the first experimental observation of the vibrational modes of imidazolyl.

We have also measured the gas phase acidity of imidazole using a FA-SIFT. From the gas phase acidity and the EA of imidazolyl, we have derived the N−H BDE of imidazole for the first time using a thermochemical cycle. The N−H BDE is a fundamental physical property of imidazole, which may be useful in understanding the thermodynamics of biological reactions of histidine. The O−H BDE of phenol in tyrosine is essential to the discussion of catalysis in photosystem II.[11]

We first present the photoelectron spectrum of imidazolide. Electronic structure calculations at the B3LYP/6-311++G(d,p) level of density functional theory (DFT) have been performed for the analysis of the spectrum. Franck−Condon simulation based on the results of the DFT calculations satisfactorily explains the main features of the spectrum. Appearance of overtone peaks of a nontotally symmetric mode is attributed to Fermi resonance. We have also observed the photoelectron spectrum of an imidazolide isomer. This isomer has been identified to be a C5 deprotonated species. Gas phase acidity measurements for imidazole are presented next. These experimental findings are discussed in the final section.

Experimental Methods

Negative Ion Photoelectron Spectroscopy. Ultraviolet negative ion photoelectron spectra of imidazolide have been obtained with a photoelectron spectrometer that has been described in detail previously,[45−47] but a brief overview is given here. Atomic oxygen anion (O^-) is formed by microwave discharge of He buffer gas (~0.5 Torr) in the presence of a trace amount of oxygen in a flowing afterglow source. The O^- reacts with methane to produce hydroxide anion (HO^-). Imidazole (Sigma, 99%) is introduced downstream via a stream of helium flowing through a crystalline sample heated to ~50 °C. The HO^- deprotonates imidazole to generate imidazolide anion. Collisions with the helium buffer gas thermalize the ions. The anions are extracted from the flowing afterglow region, accelerated to 736 eV, and focused for mass selection into a Wien velocity filter. The mass selected ions are refocused, decelerated to 35 eV, and crossed with a 351.1 nm photon beam from a cw argon ion laser in an external build-up cavity with a circulating power of approximately 100 W. A typical imidazolide beam current is 150 pA. Photoelectrons collected in a direction perpendicular to the ion and laser beams are focused, passed through a hemispherical energy analyzer with 8−12 meV resolution, and imaged onto a position sensitive detector. Spectra are obtained by measuring photoelectron counts as a function of electron kinetic energy (eKE). Subtraction of the eKE from the laser photon energy (3.531 eV) sets the energy scale of the spectra to electron binding energy (eBE). Calibration of the absolute energy scale is made with the known EA of I atom[48,49] in the measurements of the photoelectron spectrum of iodide anion. Also, the energy scale is corrected for an energy compression factor determined by measuring the photoelectron spectra of O^- and S^- in addition to I^-. A rotatable half-wave plate is inserted into the laser path before the build-up cavity to change the angle (θ) between the electric field vector of the laser beam and the photoelectron collection axis. Photoelectrons have angular distributions according to[50]

$$I(\theta) = \frac{\sigma_o}{4\pi}[1 + \beta P_2(\cos\theta)] \quad (1)$$

where σ_0 is the total photodetachment cross section, β is the anisotropy parameter, and $P_2(\cos\theta)$ is the second Legendre polynomial. The measurements at the magic angle (54.7°) provide spectra free from the angular dependence. The anisotropy parameter was determined by measurements of the photoelectron counts at $\theta = 0$ and 90°.

Flowing Afterglow-Selected Ion Flow Tube (FA-SIFT) Measurements. The gas phase acidity of imidazole has been measured using a tandem FA-SIFT instrument that has also been described previously.[51,52] To establish the acidity of imidazole, the forward (k_f) and reverse (k_r) rate constants were measured at 298 K for proton transfer reactions between imidazole ($C_3H_4N_2$) and a reference acid, 2-methyl-2-propanethiol [$(CH_3)_3$-CSH]. The ratio of the rate constants gives the proton transfer equilibrium constant K_{equil} ($\equiv k_f/k_r$).

$$C_3H_3N_2^- + (CH_3)_3CSH \underset{k_r}{\overset{k_f}{\rightleftharpoons}} C_3H_4N_2 + (CH_3)_3CS^- \quad (2)$$

The reactant anions [$C_3H_3N_2^-$ or $(CH_3)_3CS^-$] are generated in the source flow tube using hydroxide deprotonation of the corresponding neutrals. The ions are mass selected and injected into the second flow tube at low injection energies in order to minimize fragmentation. The reactant anions are thermally equilibrated with the helium buffer gas (0.5 Torr) before undergoing proton transfer reactions with an added neutral reagent. Depletion of the reactant ion signal is recorded with the detection quadrupole mass filter, and the reaction rate constants were determined.[51,52] The acidity of imidazole is determined from the equilibrium constant via the expression:

$$\Delta_{acid}G_{298}(C_3H_4N_2) = \Delta_{acid}G_{298}[(CH_3)_3CSH] + RT\ln K_{equil} \quad (3)$$

Here, $\Delta_{acid}G_{298}[(CH_3)_3CSH] = 346.2 \pm 0.2$ kcal mol^{-1} is derived from a proton transfer equilibrium constant between $(CH_3)_3CSH$ and H_2S[53] with a precise acidity of H_2S recently determined by threshold ion-pair production spectroscopy.[54,55] For the forward reaction of $C_3H_3N_2^- + (CH_3)_3CSH$, the neutral reagent is added through each of the multiple inlets located downstream along the flow tube. Depletion of the $C_3H_3N_2^-$ ion signal is measured as a function of the inlet position, i.e., the reaction distance. The measured (overall) rate constant is reproducible to within 5% (one standard deviation). The rate constant also has absolute (systematic) error bars of ±20%. In this reaction, significant adduct formation occurs concurrently with proton transfer. The branching ratio of proton transfer to adduct formation is accurately determined after correction for mass discrimination effects between the two products, $(CH_3)_3CS^-$

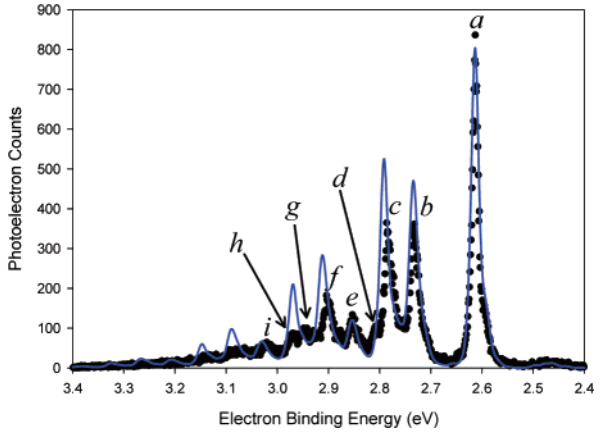

Figure 1. Magic angle photoelectron spectrum (351.1 nm) of imidazolide anion. The points are the experimental data, and the blue curve is a 15 meV fwhm Franck−Condon simulation based on the optimized geometries and normal modes obtained from the B3LYP/6-311++G(d,p) calculations.

and $[C_3H_3N_2^-\cdot(CH_3)_3CSH]$. The relative detection sensitivity is determined by back-to-back measurements of isomeric reactions: imidazolide anion + $(CH_3)_3CSH$ vs pyrazolide anion + $(CH_3)_3CSH$. The latter reaction is sufficiently exoergic and produces the proton transfer product quantitatively with respect to the depletion of the reactant anion.[56] The rate constant for proton transfer is determined from the overall rate constant and branching ratio.

In the reverse reaction of $C_3H_4N_2$ + $(CH_3)_3CS^-$, a solid sample of imidazole is heated to about 50 °C and sublimed into a stream of helium at a regulated but unknown concentration. The imidazole/He mixture is then introduced into the SIFT flow tube for subsequent reaction. Calibration of the imidazole concentration and measurement of the reverse rate constant is performed as follows: Given a constant flow of imidazole in the second flow tube, semilogarithmic depletions are measured alternately for SIFT-injected HO^- and $(CH_3)_3CS^-$ ions in order to extract the relative reaction rates. On the basis of an assumption that the exoergic proton transfer reaction between imidazole and HO^- proceeds at 90% efficiency with respect to the calculated collision rate constant (5.05×10^{-9} cm^3 s^{-1}), the absolute rate coefficient for imidazole + $(CH_3)_3CS^-$ is determined. This assumption is justified by a separate measurement of an analogous reaction of pyrrole + HO^- ($k = 2.66 \pm 0.04 \times 10^{-9}$ cm^3 s^{-1}) in comparison with the calculated collision rate constant (2.95×10^{-9} cm^3 s^{-1}). The uncertainty in the imidazole + $(CH_3)_3CS^-$ reaction rate constant is estimated from the uncertainties in the measurement/calibration procedures and in the evaluation of the collision rate constants.

The collision rate constants for imidazole and pyrrole are calculated using the parametrized trajectory collision rate theory[57] from the polarizabilities[58] of 7.15×10^{-24} and 8.03×10^{-24} cm^3 and electric dipole moments[59] of 3.8 and 1.74 D, respectively. The collision rate constant for the forward reaction is similarly calculated from the polarizability (11.2×10^{-24} cm^3)[58] and dipole moment (1.66 D)[59] of $(CH_3)_3CSH$. These rate constants are used to compute the reaction efficiencies.

Results

Photoelectron Spectra. The 351.1 nm (3.531 eV) magic angle photoelectron spectrum of imidazolide is shown in Figure 1 (solid points). The most intense peak (peak a) is assigned as the band origin, and the EA of imidazolyl is determined to be 2.613 ± 0.006 eV. Several peaks are observed to higher eBE,

TABLE 1: Peak Positions and Assignments for Photoelectron Spectrum of Imidazolide

peak[a]	peak position (cm^{-1})[b]	assignment[c]
a	0	0_0^0
b	955 ± 15	6_0^1
c	1365 ± 20	3_0^1 [d]
d	1575 ± 30	18_0^2 [d]
e	1925 ± 25	6_0^2
f	2325 ± 30	$3_0^1 6_0^1$
g	2695 ± 45	3_0^2 [e]
h	2890 ± 55	$3_0^1 18_0^2$ [e]
i	3265 ± 50	$3_0^1 6_0^2$

[a] Peak labels used in Figure 1. [b] Relative to the origin (peak a). [c] See Figure 2 for schematic representation of the normal modes. [d] Fermi resonance pair. [e] Fermi resonance pair.

TABLE 2: B3LYP/6-311++G(d,p) Optimized Geometries for Imidazolide and Imidazolyl[a]

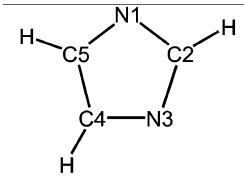

	imidazolide	imidazolyl		
	$^1A_1$	$^2B_1$	$^2B_2$	$^2A_2$
N1−C2 and N3—C2	1.3489	1.3717	1.3320	1.3398
N1−C5 and N3—C4	1.3708	1.3172	1.3794	1.4428
C4−C5	1.3917	1.4744	1.3634	1.3383
C2—H	1.0860	1.0816	1.0751	1.0804
C4−H and C5—H	1.0847	1.0825	1.0765	1.0779
∠N1-C2-N3	116.30	116.03	105.61	115.31
∠C2-N1-C5 and ∠C2-N3-C4	102.69	103.10	111.23	103.64
∠N1-C5-C4 and ∠N3-C4-C5	109.16	108.88	105.96	108.70
∠N1-C2-H and ∠N3-C2-H	121.85	121.98	127.20	122.35
∠N1-C5-H and ∠N3-C4-H	121.65	123.00	121.05	119.98

[a] Bond lengths are in units of Å, and bond angles are in units of degrees.

representing vibrational levels of imidazolyl. Table 1 gives the energies of the observed peaks relative to the origin. Angular distributions of photoelectrons have been measured, and the anisotropy parameter (β) for the main peaks is about −0.3.

DFT calculations were performed to make assignments of the photoelectron spectrum. Becke's hybrid three-parameter functional[60] and the correlation functional of Lee, Yang, and Parr[61] (B3LYP) were employed with the 6-311++G(d,p) basis set.[62] Harmonic vibrational frequencies were calculated at stationary points obtained by geometry optimizations and are used without scaling. All of the calculations were carried out with the Gaussian 03 suite of programs.[63]

The DFT calculations predict that the electronic ground state of imidazolide is $^1A_1$, while the ground state of imidazolyl is $^2B_1$. The optimized geometries are given in Table 2, and the harmonic vibrational frequencies are shown in Table 3. Using these results, Franck−Condon factors were calculated for transitions from the $^1A_1$ imidazolide to the $^2B_1$ imidazolyl with the PESCAL program.[64,65] Figure 1 shows a 15 meV fwhm Gaussian line shape convolution (blue line) of the raw Franck−Condon factors. The simulation reproduces the observed spectrum reasonably well. The DFT calculations also predict

TABLE 3: B3LYP/6-311++G(d,p) Harmonic Vibrational Frequencies (cm^{-1}) for $\tilde{X}\ ^1A_1$ Imidazolide and $\tilde{X}\ ^2B_1$ Imidazolyl[a]

mode	symmetry	imidazolide	imidazolyl
1	a_1	3172	3231
2		3147	3218
3		1443	1436
4		1254	1313
5		1184	1166
6		1086	982
7		935	919
8	a_2	777	874
9		666	560
10	b_1	809	867
11		734	756
12		696	511
13	b_2	3145	3205
14		1466	1523
15		1304	1289
16		1231	1188
17		1100	1016
18		931	780

[a] Frequencies are unscaled.

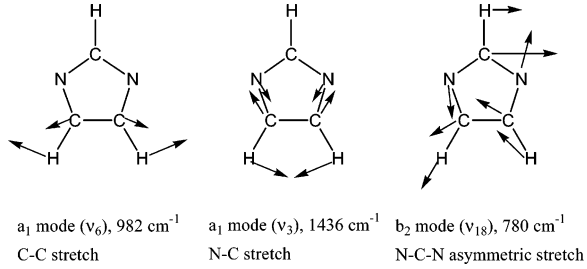

Figure 2. Relative atomic displacements and harmonic frequencies of the normal modes for $\tilde{X}\ ^2B_1$ imidazolyl evaluated at the B3LYP/6-311++G(d,p) level of theory.

an EA of 2.592 eV, which is in good agreement with the experimental value. Thus, we assign the observed spectrum to the $^2B_1$ ground state of imidazolyl. This assignment is consistent with the hyperfine structures of imidazolyl radical observed in aqueous solution.[43]

The Franck−Condon simulation allows assignments of the observed vibrational peaks. The first vibrational peak (peak b) is a totally symmetric (a_1) C−C stretching mode (ν_6). The next peak (peak c) is another a_1 mode with N−C stretching motion (ν_3). Atomic displacements for these normal modes obtained from the DFT calculations are schematically depicted in Figure 2. The overtone of the C−C stretching mode ($2\nu_6$) and the combination of the C−C stretching and N−C stretching modes ($\nu_3 + \nu_6$) appear in the spectrum as peaks e and f, respectively. Even though the main features of the spectrum are reproduced satisfactorily, there are some discrepancies between the observed spectrum and the Franck−Condon simulation. For example, a small shoulder to the higher eBE side of peak c is observed (peak d). This feature is absent in the Franck−Condon simulation. The intensity of ν_3 (peak c) is overestimated in the simulation, so are $\nu_3 + \nu_6$ (peak f) and $2\nu_3$ (peak g). Furthermore, the vibrational frequency of ν_3 is overestimated in the DFT calculations, while the DFT frequency of ν_6 matches the observed vibrational energy level very well.

Reviewing the DFT harmonic frequencies for $^2B_1$ imidazolyl in Table 3, peak d may correspond to the overtone of either a b_1 mode ($2\nu_{11}$) or a b_2 mode ($2\nu_{18}$). Even quanta of nontotally symmetric modes are symmetry-allowed, and they can be observed in the spectrum. Generally, a nonzero Franck−Condon factor for these overtones originates from a large change in the corresponding vibrational frequencies between the initial and the final states of the electronic transition. In the imidazolide system, however, there is no significant Franck−Condon factor for either $2\nu_{11}$ or $2\nu_{18}$, as can be seen in the simulation in Figure 1.

TABLE 4: Cubic Force Constants (cm^{-1}) for $\tilde{X}\ ^2B_1$ Imidazolyl and Geometry Displacement Parameters, *K*, in Dimensionless Normal Coordinates for $\tilde{X}\ ^2B_1$ Imidazolyl − $\tilde{X}\ ^1A_1$ Imidazolide, and $\tilde{X}\ ^2B_1$ − $(\tilde{B})\ ^2A_2$ Imidazolyl Evaluated at the B3LYP/6-311++G(d,p) Level of Theory

a_1 mode *i*	$\Phi_{i,11,11}$	$\Phi_{i,18,18}$	$K\ (^2B_1 - {}^1A_1)$	$K\ (^2B_1 - {}^2A_2)$
1	148	10	0.036	0.075
2	758	7	0.031	0.081
3	25	209	1.249	2.768
4	33	44	0.376	1.094
5	23	48	0.322	0.026
6	18	100	0.919	1.488
7	8	58	0.534	1.322

Alternatively, overtone peaks can gain intensity from Fermi resonance.[66] The Fermi resonance mixes two vibrational levels of the same vibrational symmetry, and the extent of mixing is larger when the energy separation of the two unperturbed vibrational levels is smaller. Peak d is located very close to peak c whose Franck−Condon factor is very large according to the simulation. The two peaks are separated by only ~200 cm^{-1}. The mixing of the two levels takes place through anharmonic coupling. DFT methods have recently been applied to a number of molecules for anharmonic calculations.[67−70] Numerical differentiation of the analytic second derivatives is implemented in Gaussian 03 program package[63] to obtain cubic force constants. The cubic force constants for the $^2B_1$ imidazolyl are calculated at its stationary point with respect to Cartesian coordinates, and they are transformed into the basis of the dimensionless normal coordinates. Table 4 shows cubic force constants involving the a_1 modes and ν_{11} or ν_{18}. The calculated cubic force constants for (ν_3, ν_{18}, ν_{18}) and (ν_3, ν_{11}, ν_{11}) are 209 and 25 cm^{-1}, respectively. A simple 2×2 matrix is set up for each anharmonic coupling to evaluate the corresponding Fermi resonance mixing, using the DFT harmonic frequencies. The mixing between ν_3 and $2\nu_{18}$ is about 10%, and the concomitant energy shift is 19 cm^{-1}. On the other hand, the mixing of ν_3 and $2\nu_{11}$ is less than 1%, and the energy shift is less than 1 cm^{-1}. These DFT calculations suggest that the Fermi resonance effects are much larger for ν_3 and $2\nu_{18}$ despite the larger separation of the energy levels. Therefore, we propose that peak d is $2\nu_{18}$, borrowing intensity from the Franck−Condon factor of ν_3 (peak c) through the Fermi resonance. Likewise, the Fermi resonance effects operate for peaks g and h, which correspond to $2\nu_3$ and $\nu_3 + 2\nu_{18}$, respectively.

To the lower eBE side of the origin peak a in Figure 1, weak photoelectron signals are detected as shown in Figure 3. The intensity of these photoelectron signals is much lower (<1%) than that of peak a in Figure 1, whose leading edge appears in Figure 3. The peak at ~2.45 eV has been identified as an 1165 ± 45 cm^{-1} hot band of imidazolide, whose vibrational temperature is about 450 K. This hot band of broad line width consists of several totally symmetric modes of imidazolide (see Table 3). However, the other peaks apparent in Figure 3 cannot be hot bands of imidazolide. The assignment of the $\tilde{X}\ ^2B_1$ state of imidazolyl in Figure 1 is well-established, as described above. Therefore, the photoelectrons observed at lower eBE than those for the $\tilde{X}\ ^2B_1$ state cannot originate from 1-imidazolide anion. When O^- was used instead of HO^- as a reactant in the flow tube to synthesize imidazolide anion, we detected the photo-

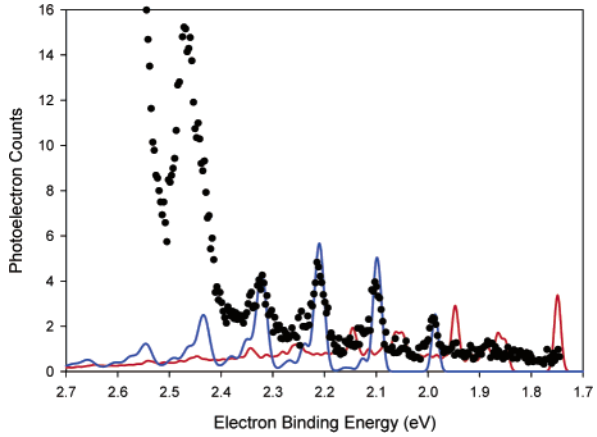

Figure 3. Portion of the 351.1 nm magic angle photoelectron spectrum of the anions produced from the imidazole + HO^- reaction. The solid points are the experimental data, the blue curve is simulation of 5-imidazolide detachment, and the red curve is simulation of 2-imidazolide detachment. The Franck−Condon simulation (15 meV fwhm) uses the EAs, optimized geometries, and normal modes obtained from the B3LYP/6-311++G(d,p) calculations. The peak at ~2.45 eV is the hot band of imidazolide, and the intense origin peak of 1-imidazolide grows in at >2.5 eV.

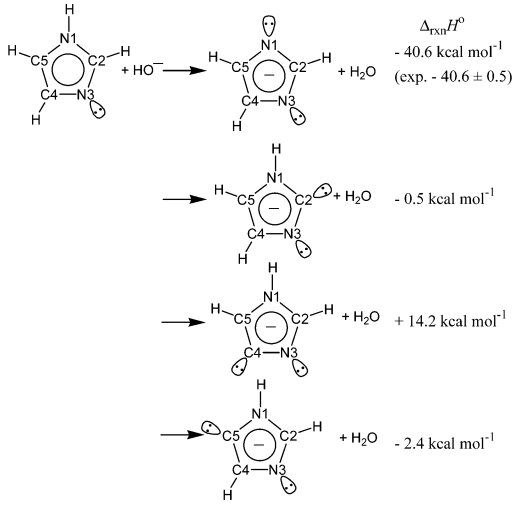

Figure 4. B3LYP/6-311++G(d,p) reaction enthalpies for proton transfer reactions at different positions of imidazole. A literature value is used for the deprotonation enthalpy of H_2O (see ref 55).

electron spectrum of imidazolide, virtually identical with that shown in Figure 1; however, the peaks as shown in Figure 3 were not observed. Because HO^- is a stronger base than O^-,[71] it is possible that deprotonation of imidazole may take place not only at the nitrogen site but also at a less acidic carbon site when HO^- is used. In this case, detachment from the carbon-deprotonated anion may lead to the observation of the photoelectron spectrum in Figure 3.

The energetics of deprotonation at all sites of imidazole was explored with DFT calculations, and the results are shown in Figure 4. The DFT calculations predict $\Delta_{acid}H_{298}$ to be 349.6 kcal mol^{-1} for the N1 position, in excellent agreement with an experimental value of 349.7 ± 0.5 kcal mol^{-1} (vide infra). Combined with a reported deprotonation enthalpy of H_2O ($\Delta_{acid}H_{298}$ = 390.27 ± 0.03 kcal mol^{-1}),[55] the enthalpy of HO^- reaction with imidazole to yield imidazolide and H_2O is calculated to be −40.6 kcal mol^{-1} (cf. experimental value is −40.6 ± 0.5 kcal mol^{-1}). The DFT calculations find the other protons in imidazole to be much less acidic. The calculated deprotonation enthalpies, $\Delta_{acid}H_{298}$, are 389.8, 404.4, and 387.9 kcal mol^{-1} for the C2, C4, and C5 positions, respectively. As shown in Figure 4, HO^- deprotonation of imidazole is slightly exothermic at C2 and C5, but it is quite endothermic for C4 deprotonation. The deprotonation enthalpy of hydroxyl radical[71] is $\Delta_{acid}H_{298}$ = 382.70 ± 0.10 kcal mol^{-1}, and the DFT calculation results suggest that deprotonation at all of the carbon sites of imidazole by O^- is endothermic.

TABLE 5: B3LYP/6-311++G(d,p) Optimized Geometries for 5-Imidazolide and 5-Imidazolyl[a]

	5-imidazolide $^1A_1$	5-imidazolyl $^2A•$
N1−C2	1.3766	1.3683
C2 N3	1.3166	1.3154
N3−C4	1.3960	1.3843
C4−C5	1.3996	1.3630
C5−N1	1.4056	1.3701
N1−H	1.0066	1.0074
C2−H	1.0839	1.0791
C4−H	1.0841	1.0759
∠N1-C2-N3	110.36	111.12
∠C2-N3-C4	103.94	107.20
∠N3-C4-C5	114.96	107.47
∠C4-C5-N1	98.95	108.51
∠C5-N1-C2	111.79	105.71
∠H-N1-C2	124.54	127.83
∠H-C2-N1	123.75	123.22
∠H-C4-C5	126.34	129.98

[a] Bond lengths are in units of Å, and bond angles are in units of degrees.

Franck−Condon simulations for photodetachment from 2-imidazolide and 5-imidazolide were carried out, and the results are shown in Figure 3. The DFT calculations predict the ground states of the corresponding radicals to be σ states ($^2A'$) with EAs of 1.749 and 1.986 eV for 2-imidazolyl and 5-imidazolyl, respectively. It is evident that the Franck−Condon profiles for the two species are quite distinct and that the simulation for 5-imidazolide is in excellent agreement with the observed spectrum. Thus, it is concluded that a minor pathway of HO^- reaction with imidazole is deprotonation at the C5 position, and photodetachment from 5-imidazolide leads to the formation of $\tilde{X}\ ^2A'$ state of 5-imidazolyl radical, which appears in Figure 3. The DFT optimized geometries of the anion and the radical are given in Table 5. The Franck−Condon simulation helps to identify the origin peak, and the EA of 5-imidazolyl is determined to be 1.992 ± 0.010 eV. An extensive vibrational progression with a frequency of 900 ± 70 cm^{-1} is observed in the spectrum. The simulation predicts that two in-plane ring bending modes with harmonic frequencies of 859 and 931 cm^{-1} are active in the photoelectron spectrum. This vibrational progression reflects large differences in the angles of the five-membered ring between the ground states of the anion and the neutral, particularly the ∠C4−C5−N1 angle (Table 5).

Gas Phase Acidity. For reactions of imidazolide with $(CH_3)_3$-CSH and imidazole with $(CH_3)_3CS^-$, the overall rate constants ($k_{overall}$) including proton transfer and adduct formation were measured to be 3.04 ± 0.61 × 10^{-10} cm^3 s^{-1} and 2.60 ± 0.70

TABLE 6: Thermochemical Parameters for Imidazole and Imidazolyl[a]

EA (imidazolyl)[b]	2.613 ± 0.006 eV
$\Delta_{acid}G_{298}$(imidazole)[b]	342.6 ± 0.4 kcal mol^{-1}
$\Delta_{acid}G_{298}$(imidazole)[c]	342.8 ± 2.0 kcal mol^{-1}
$\Delta_{acid}S_{298}$(imidazole)[d]	23.8 cal mol^{-1} K^{-1}
$\Delta_{acid}H_{298}$(imidazole)[e]	349.7 ± 0.5 kcal mol^{-1}
$\Delta_{acid}H_{0}$(imidazole)[f]	348.4 ± 0.5 kcal mol^{-1}
D_0(imidazole)[g]	95.1 ± 0.5 kcal mol^{-1}
Δ_fH_{298}(imidazolyl)[h]	76.2 ± 0.6 kcal mol^{-1}

[a] Acidities and bond enthalpies are associated with the N−H hydrogen and N−H bond, respectively. [b] Experimentally determined in the present study. [c] Ref 72. [d] Derived from DFT calculation [B3LYP/6-311++G(d,p)] using unscaled vibrational frequencies. [e] Derived from $\Delta_{acid}G_{298}$(imidazole) and thermal correction. [f] Derived from $\Delta_{acid}H_{298}$-(imidazole) and thermal correction. [g] Determined with EA(imidazolyl) and $\Delta_{acid}H_0$(imidazole) through a thermochemical cycle (see eq 7 in the text). [h] Derived from Δ_fH_{298}(imidazole) and D_0(imidazole) and thermal corrections (see eq 8 in the text).

× 10^{-9} cm^3 s^{-1}, respectively, where the uncertainties represent absolute error bars. Not only is the overall reaction of imidazolide with $(CH_3)_3CSH$ slower than the reverse reaction, but it proceeds primarily via adduct formation (≈98%). This indicates that the forward direction is endoergic in the proton transfer equilibrium. Using a reasonable assumption that the adducts originate from the endoergic fraction of the Boltzmann thermal energy distribution, the overall rate constant can be partitioned into the effective rate constant for proton transfer, $k_f = 6.4 \pm 1.9 \times 10^{-12}$ cm^3 s^{-1}, with the uncertainty representing both the absolute error bars in the overall rate measurement and the counting statistics of the minor proton transfer product. The proton transfer efficiency is only 0.35% with respect to the collision rate constant of 1.83 × 10^{-9} cm^3 s^{-1}.

As discussed above, a very small amount of 5-imidazolide anion was observed as a minor product of HO^- deprotonation of imidazole in the photoelectron spectroscopic measurements. Assuming an identical photodetachment cross-section for the two isomers, 1-imidazolide and 5-imidazolide, the amount of 5-imidazolide produced in the photoelectron spectroscopic apparatus would be less than 1% of 1-imidazolide anions. If a significant portion of *m*/*z* 67 ions were 5-imidazolide in the SIFT apparatus, then analysis of ion reaction with $(CH_3)_3CSH$ would need to take account of the isomer contamination.

Our experimental findings, however, indicate that formation of 5-imidazolide in the SIFT apparatus is negligible. Collision-induced dissociation (CID) of imidazole was performed by increasing the ion injection energy and observing the fragmentation upon collision with helium in the second flow tube. The CID measurements used the same condition for the ion formation in the flowing afterglow source as the kinetics measurements. The CID energy dependence shows no evidence for the 5-imidazolide isomer, which is nearly 40 kcal mol^{-1} higher in energy than 1-imidazolide (see Figure 4). On the basis of the detection sensitivity, the upper bound is estimated to be 3% for the abundance of 5-imidazolide.

Kinetics measurements for the imidazolide + $(CH_3)_3CSH$ reaction also show no sign of the presence of 5-imidazolide. While 5-imidazolide anions are expected to deprotonate $(CH_3)_3$-CSH at nearly every collision (1.83 × 10^{-9} cm^3 s^{-1}), ~6 times faster than the observed overall decay (3.04 × 10^{-10} cm^3 s^{-1}), there was no faster decaying component in the imidazolide depletion plot nor prompt formation of the product ion, $(CH_3)_3CS^-$, in the early stage of the kinetics. The rate of formation of $(CH_3)_3CS^-$ was constant over the entire course of the reaction kinetics well beyond the time scale for 5-imidazolide depletion. Thus, the assigned rate constant (6.4 ± 1.9 × 10^{-12} cm^3 s^{-1}) must represent exclusively the proton transfer reaction between 1-imidazolide and $(CH_3)_3CSH$.

The reverse reaction of imidazole with $(CH_3)_3CS^-$ proceeds exclusively via proton transfer (>99%) with negligible adduct formation. The proton transfer rate constant is essentially the same as the overall, $k_r = 2.60 \pm 0.70 \times 10^{-9}$ cm^3 s^{-1}. The reaction efficiency amounts to 87% of the collision rate constant (3.00 × 10^{-9} cm^3 s^{-1}). The gas phase acidity difference, $\Delta\Delta_{acid}G_{298}$[imidazole − $(CH_3)_3CSH$], is derived from the forward and reverse rate constants as −3.6 ± 0.3 kcal mol^{-1}. Because $\Delta_{acid}G_{298}[(CH_3)_3CSH] = 346.2 \pm 0.2$ kcal mol^{-1}, the gas phase acidity, $\Delta_{acid}G_{298}$(imidazole), is determined as 342.6 ± 0.4 kcal mol^{-1}. This experimental value of the gas phase acidity of imidazole is in excellent agreement with a previous FT-ICR measurement[72,73] of 342.8 ± 2.0 kcal mol^{-1}, which incorporates recent changes in the acidity scale.[71] Table 6 summarizes the thermochemical information determined for imidazole and imidazolyl.

Discussion

Electronic Structure of $^2B_1$ Imidazolyl. As mentioned in the Introduction, our research is directed at understanding how successive substitution of an N atom for a C−H group affects the properties of five-membered cyclic compounds. Previously, we studied pyrrolide anion and the corresponding radical, pyrrolyl, which have one N atom in the ring.[8] The C_2 axis of pyrrolide and pyrrolyl runs through the N atom. Of the two highest occupied molecular π-orbitals, the b_1 orbital has a large contribution from the N p orbital, while the a_2 orbital has no direct contributions from the N p orbital because the N atom lies on the π-node. The N atom participation stabilizes the b_1 orbital, which explains that the ground state of pyrrolyl is the $^2A_2$ state. The term energy of the $^2B_1$ state is expected to be ~0.5 eV although it is a transition state due to the strong vibronic coupling with the $^2A_2$ state.[8]

With the arrangement of the two N atoms, the C_2 axis runs through the C2 atom for imidazolide and imidazolyl. Consequently, the a_2 orbital is mainly composed of the N p orbitals, but the b_1 orbital has only minor contributions from the N p orbitals (see Figure 5). Thus, the a_2 orbital is more stabilized than the b_1 orbital in imidazolide. Photodetachment from the highest occupied molecular orbital (i.e., b_1 orbital) leads to the formation of the $^2B_1$ ground state of imidazolyl. The angular distribution parameter, β, was found to be −0.3 for the main features of the $^2B_1$ imidazolyl (Figure 1). A negative β value is typical for photoelectrons in this range of kinetic energy when detachment takes place from π-molecular orbitals.[8,23,74]

Because of the large effects of the two N atoms on the a_2 orbital, the extent of stabilization of the a_2 orbital relative to the b_1 orbital in imidazolyl is much larger than the corresponding situation in the pyrrolyl system. The DFT calculations predict that the term energy of the $^2A_2$ state of imidazolyl is 0.95 eV.[75] Indeed, the lowest excited state is calculated to be a σ state, the $^2B_2$ state, with a term energy of 0.84 eV (Figure 5).[75] Either our laser photon energy is not sufficient for detachment to these excited states or the kinetic energy of the photoelectrons may be too low (<0.15 eV) for efficient detection. It should be mentioned that the DFT calculations show that the two excited states vibronically couple with each other strongly, and as a result, the corresponding C_{2v} stationary points are saddle points.

The EA increases as the number of N atoms in the five-membered ring increases. The EAs of cyclopentadienyl (C_5H_5), pyrrolyl (NC_4H_4), and imidazolyl ($N_2C_3H_3$) are 1.812 ± 0.005,[76] 2.145 ± 0.010,[8] and 2.613 ± 0.006 eV, respectively. The highest

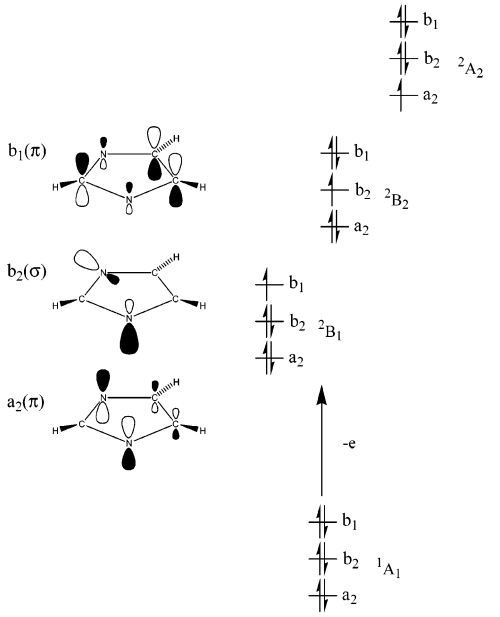

Figure 5. Three highest occupied molecular orbitals of imidazolide, and the schematic representation of electron photodetachment from imidazolide to form three electronic states of imidazolyl radical. Only $\tilde{X}\ ^2B_1$ state is observed in the photoelectron spectrum (Figure 1).

occupied molecular orbitals of pyrrolide (a_2 orbital) and imidazolide (b_1 orbital) are not mainly composed of N p orbitals. However, the inductive effects of the N atoms in the ring stabilize these orbitals significantly; hence, the EA increases with the number of N atoms.

The Franck−Condon profile of the photoelectron spectrum shown in Figure 1 reflects the geometry change from $\tilde{X}\ ^1A_1$ imidazolide to $\tilde{X}\ ^2B_1$ imidazolyl. In Table 2, the most noticeable change between the two equilibrium geometries is the N1−C5 (or equivalently N3−C4) bond length and the C4−C5 bond length. Indeed, the two a_1 modes active in the photoelectron spectrum (ν_3 and ν_6) are the N−C stretching mode and the C−C stretching mode, as shown in Figure 2.

The appearance of $2\nu_{18}$ and its combination band (peaks d and h) was attributed to Fermi resonance with ν_3. This Fermi resonance, at least to some extent, explains the discrepancies between the observed spectrum and the Franck−Condon simulation. It should be remembered that our Franck−Condon simulation was carried out with a harmonic assumption; that is, it does not take into account anharmonic effects, such as Fermi resonance. As noted in the results section, the intensity of ν_3 (peak c) is overestimated in the Franck−Condon simulation. When ν_3 is in Fermi resonance with $2\nu_{18}$, their characters are mixed. With the cubic force constant in Table 4, the extent of mixing is calculated to be 10%. Because $2\nu_{18}$ does not have an appreciable Franck−Condon factor in the absence of the Fermi resonance, this mixing should result in the decrease of intensity for ν_3, while $2\nu_{18}$ gains intensity from ν_3. Thus, the discrepancy in the peak c intensity between the simulation and the observed spectrum in Figure 1 should be reduced by the anharmonic effects. In addition, with the energy ordering of ν_3 and $2\nu_{18}$ as found in the DFT calculations (see Table 3), the Fermi resonance lowers the ν_3 energy level, while $2\nu_{18}$ is raised. Lowering of ν_3 also alleviates the discrepancy found between the DFT harmonic frequency and the observed peak position. The same logic applies to the overestimation of the intensities as well as the energy levels of peak f ($\nu_3 + \nu_6$) and peak g ($2\nu_3$). The Fermi resonance coupling matrix element is larger for higher vibrational quantum numbers. Thus, $2\nu_3$ (peak g) and $\nu_3 + 2\nu_{18}$ (peak h) will have even stronger mixing than ν_3 (peak c) and $2\nu_{18}$ (peak d), which could explain comparable intensities for peaks g and h. It should be noted that the DFT frequency of ν_6 reproduces the observed peak position (peak b) very well. This C−C stretch fundamental is not expected to have any significant Fermi resonance effects.

Table 4 shows cubic force constants for ν_{18} (quadratic) and each a_1 mode (linear) of imidazolyl. A particularly large cubic force constant is found for ν_3, $\Phi_{3,18,18} = 209\ cm^{-1}$, which is much larger than the second largest one, $\Phi_{6,18,18} = 100\ cm^{-1}$. This large magnitude of the anharmonicity, $\Phi_{3,18,18}$, may be related to vibronic coupling between the $^2B_1$ and the $^2A_2$ states. The Herzberg−Teller expansion up to second-order is[77]

$$V_i = V_0 + \sum_\alpha \left\langle \Psi_i \left| \frac{\partial H}{\partial Q_\alpha} \right| \Psi_i \right\rangle Q_\alpha + \frac{1}{2} \sum_\alpha \left\langle \Psi_i \left| \frac{\partial^2 H}{\partial {Q_\alpha}^2} \right| \Psi_i \right\rangle {Q_\alpha}^2 - \sum_{\alpha, k \neq i} \frac{\left\langle \Psi_i \left| \frac{\partial H}{\partial Q_\alpha} \right| \Psi_k \right\rangle \left\langle \Psi_k \left| \frac{\partial H}{\partial Q_\alpha} \right| \Psi_i \right\rangle}{E_k - E_i} {Q_\alpha}^2 \quad (4)$$

Here, the reference is taken at a C_{2v} geometry. The last term represents the vibronic coupling effects on the quadratic force constants. For the vibronic coupling between the $^2B_1$ and the $^2A_2$ states, normal modes of b_2 symmetry will make nonzero matrix elements in the last term. When the potential energy surface of the $^2B_1$ state is expressed in this expansion form, it is evident that the effects of vibronic coupling on the $^2B_1$ potential energy surface near its equilibrium geometry are marginal because of the relatively large denominator in the last term. The DFT calculations show that the $^2A_2$ state lies 1.9 eV higher in energy than the $^2B_1$ state at the $^2B_1$ equilibrium geometry.

The large cubic force constant, $\Phi_{3,18,18}$, is explicitly written as

$$\Phi_{3,18,18} = \frac{\partial^3 V}{\partial Q_3\, \partial Q_{18}\, \partial Q_{18}} = \frac{\partial}{\partial Q_3} \left(\frac{\partial^2 V}{\partial {Q_{18}}^2} \right) \quad (5)$$

This cubic force constant is a gradient of the quadratic force constant for the b_2 mode, ν_{18}, along the totally symmetric mode, ν_3. As seen in eq 4, the ν_{18} quadratic force constant depends on the vibronic coupling between the $^2B_1$ and the $^2A_2$ states. Consequently, the cubic force constant, $\Phi_{3,18,18}$, can exhibit the dependence of the vibronic coupling on the ν_3 motion.

In the Franck−Condon simulation shown in Figure 1, the parameters of the following equation are calculated[78]

$$Q = JQ' + K \quad (6)$$

Here, Q' and Q are matrices for the normal coordinates of the imidazolide and imidazolyl ground states, respectively, J is a matrix for Duschinsky rotation of the two sets of normal coordinates, and K is a column vector representing the geometry displacement between the two states. The components of the K vector for all of the a_1 modes of the $^2B_1$ imidazolyl are shown in Table 4. The largest displacement takes place along ν_3, and the magnitude of the displacement is 1.249 in dimensionless units. The second largest value is ν_6, 0.919. These large displacements manifest themselves in the photoelectron spectrum (Figure 1) as vibrational progression for these modes.

In the same way, the K vector can be calculated for the geometry shift from the $^2B_1$ ground state to the $^2A_2$ excited state of imidazolyl, and its components are shown in Table 4. The

geometry shift along ν_3 is by far the largest, 2.768, between the two imidazolyl states. The large *K* vector component for the N−C stretching mode is not surprising as Table 2 shows that the N1−C5 (N3−C4) bond length is quite different between the $^2B_1$ and the $^2A_2$ states. Let us assume that the $^2B_1$ and $^2A_2$ states have identical normal modes (i.e., parallel modes) and that the potential energy surface is harmonic. Then, the *K* vector represents the slopes of the $^2A_2$ potential energy surface along the a_1 modes at the equilibrium geometry of the $^2B_1$ state. Under this assumption, the energy separation between the $^2B_1$ and the $^2A_2$ states changes by ~0.6 eV as the geometry shifts along the ν_3 mode by one dimensionless unit. Figure 2 shows the schematic representation of the ν_{18} mode. This mode is asymmetric NCN stretching. The corresponding mode in pyrrolyl was found to be responsible for strong vibronic coupling between the $^2A_2$ and the $^2B_1$ states.[8] Taking the magnitude of the vibronic coupling matrix as 0.15 eV, which represents moderately strong vibronic coupling,[79−83] the quadratic coupling constant for the ν_{18} mode of imidazolyl changes by 90 cm^{-1} as the energy separation decreases from 1.9 to 1.3 eV. Thus, it is reasonable that the vibronic coupling between the $^2B_1$ and the $^2A_2$ states contributes to the relatively large anharmonicity, which causes the Fermi resonance effects.

Imidazole N−H Bond Thermodynamics. The N−H BDE of imidazole, $D_0(C_3H_3N_2-H)$, is derived in the following thermochemical cycle:

$$D_0(C_3H_3N_2-H) = \Delta_{acid}H_0(C_3H_3N_2-H) + EA(C_3H_3N_2) - IE(H) \quad (7)$$

Here, $EA(C_3H_3N_2)$ is the imidazolyl EA, $\Delta_{acid}H_0(C_3H_3N_2-H)$ is the imidazole 0 K N−H deprotonation enthalpy, and IE(H) is the ionization energy of the hydrogen atom (13.59844 eV). The experimentally determined gas phase acidity, the 298 K deprotonation free energy ($\Delta_{acid}G_{298}$), is converted to the 298 K deprotonation enthalpy ($\Delta_{acid}H_{298}$), using the deprotonation entropy evaluated from the DFT calculations: $\Delta_{acid}H_{298}$(imidazole) = 349.7 ± 0.5 kcal mol^{-1}. The 0 K deprotonation enthalpy ($\Delta_{acid}H_0$) is obtained from the 298 K deprotonation enthalpy ($\Delta_{acid}H_{298}$) by subtracting the contributions of integrated heat capacities, which are also evaluated from the DFT calculations: $\Delta_{acid}H_0$(imidazole) = 348.4 ± 0.5 kcal mol^{-1}. With this acidity value and the experimental EA value substituted in eq 7, the 0 K N−H BDE of imidazole is derived to be $D_0(C_3H_3N_2-H)$ = 95.1 ± 0.5 kcal mol^{-1}. Subsequently, the heat of formation of imidazolyl radical, $\Delta_fH_{298}(C_3H_3N_2)$, is determined from the following relation:

$$\Delta_fH_{298}(C_3H_3N_2) = \Delta_fH_{298}(C_3H_4N_2) + DH_{298}(C_3H_3N_2-H) - \Delta_fH_{298}(H) \quad (8)$$

where $\Delta_fH_{298}(C_3H_4N_2)$ is the heat of formation of imidazole and $\Delta_fH_{298}(H)$ is the heat of formation of hydrogen atom. Using thermodynamic information from the DFT calculations, the N−H BDE value from above, and a reported heat of formation of imidazole [$\Delta_fH_{298}(C_3H_4N_2)$ = 31.8 ± 0.1 kcal mol^{-1}],[71] we obtain $\Delta_fH_{298}(C_3H_3N_2)$ = 76.2 ± 0.6 kcal mol^{-1}. All thermal corrections used were computed using unscaled vibrational frequencies.

The N−H BDE of imidazole, 95.1 ± 0.5 kcal mol^{-1}, is very close to the N−H BDE of pyrrole,[84] 93.92 ± 0.11 kcal mol^{-1}. In terms of eq 7, the increase in EA from the pyrrole to the imidazole system is approximately canceled by the decrease in the acidity. There is no significant effect of the additional N atom in the five-membered ring on the N−H BDE.

As introduced earlier, elucidation of the mechanism of ALS has recently been an active research topic in the field of biological chemistry. Information on oxidative reactions in Cu,Zn−SOD is important in understanding their possible participation in the development of toxicity. The peroxidase reaction of Cu,Zn−SOD has been studied in this context.[41,85] The observation of the histidinyl radical suggests that the oxidizing agent, possibly OH radical, reacts with one of the coordinating imidazole rings of the histidines at the metal center. The OH radical reactions with pyrrole and imidazole can be expressed as formal H-atom abstraction reactions:

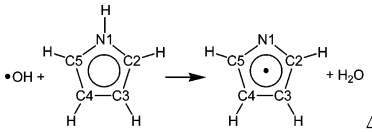

$$\Delta_{rxn}H_{298} = -23.5 \pm 0.2 \text{ kcal mol}^{-1} \quad (9)$$

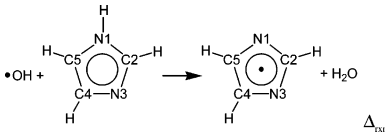

$$\Delta_{rxn}H_{298} = -22.4 \pm 0.5 \text{ kcal mol}^{-1} \quad (10)$$

With the N−H BDE of imidazole, the reported N−H BDE of pyrrole, and the O−H BDE of H_2O,[55] we can calculate the enthalpies of the two reactions, as indicated above. The two reaction enthalpies are similar and moderately exothermic. However, in aqueous solutions, the two reactions have quite different characters. In neutral aqueous solutions, the OH radical reaction with pyrrole leads to the formation of pyrrolyl radical, while the product of the OH reaction with imidazole is the OH adduct; no formation of imidazolyl is observed at pH < 10.[43,86,87] Solvation effects (e.g., hydrogen bonding) on the reactants and products are not expected to change the enthalpies of the two reactions significantly.

The most probable explanation of the difference in the two reactions is related to the charge transfer character of the reaction processes. Tripathi discussed direct electron transfer and adduct-mediated electron transfer mechanisms of OH radical reactions with aromatic compounds in his resonance Raman study.[88] He demonstrated that the electron transfer processes take place more efficiently with those aromatic compounds with lower IEs. Similarly, charge transfer from pyrrole to OH radical may be effective, considering the relatively low IE of pyrrole, 8.23 eV,[89] or alternatively, the EA of pyrrolyl, 2.145 ± 0.010 eV.[8] This charge transfer should be accompanied by deprotonation in the formation of pyrrolyl radical. On the other hand, the IE of imidazole is 8.78 eV,[89] and the EA of imidazolyl is 2.613 ± 0.006 eV. Thus, one more N atom in the ring makes removal of a negative charge from imidazole more difficult, and the OH radical simply adds to the imidazole ring. A charge transfer aspect of the OH radical reactions with aromatic compounds has also been considered in a recent kinetics study in acetonitrile solutions.[90] The OH radical reaction with imidazole has also been studied theoretically.[91]

A recent DFT study[92] shows that the N−H BDE of imidazole is calculated to be 121 kcal mol^{-1}, which is clearly erroneous. In this work, the authors apparently used a σ-state of imidazolyl as the bond dissociation asymptote. The $^2B_2$ state correlates diabatically with the ground state of imidazole as the N−H bond is stretched within the molecular plane. Adiabatically, however, the $^2B_1$ ground state of imidazolyl is the correct asymptote to derive the N−H BDE. Moreover, their acidity value differs from ours by ~7 kcal mol^{-1}, even though the same DFT method and the same basis set were used in their study. As demonstrated

earlier, our DFT value of the acidity is in excellent agreement with the experimental value. It is possible that there are some systematic errors in their derivation of thermodynamic parameters.

Imidazole C−H Bond Thermodynamics. The C−H BDE of heteroaromatic compounds is a key subject in the discussion of combustion processes[93,94] or transition metal catalysis.[95−98] Blank et al. determined the C−H BDE of pyrrole in photofragment translational spectroscopic measurements.[99] However, because the N−H BDE of pyrrole determined in the same study is not accurate (see ref 84), their value of the C−H BDE is questionable. No definitive experimental values on the C−H BDE of heteroaromatic compounds have been reported in the literature.

The photoelectron spectrum shown in Figure 3 definitively indicates that HO^- abstracts the proton at the C5 position. When the reagent was changed from HO^- to O^-, the photoelectron spectrum as shown in Figure 3 was not observed, and only the photoelectron spectrum of 1-imidazolide (Figure 1) was observed. These results could indicate that the acidity of imidazole at the C5 position is bracketed by those of H_2O and OH radical. The gas phase acidities of H_2O and OH radical are $\Delta_{acid}G_{298} = 383.68 \pm 0.02$ and 376.80 ± 0.20 kcal mol^{-1}, respectively.[55,71]

The DFT calculations predict $\Delta_{acid}G_{298} = 342.5$ kcal mol^{-1} for N−H of imidazole. This compares very well with our experimental value, $\Delta_{acid}G_{298} = 342.6 \pm 0.4$ kcal mol^{-1}. For the acidities at the carbon sites, $\Delta_{acid}G_{298} = 381.9$, 396.2, and 380.2 kcal mol^{-1} are predicted for the C2, C4, and C5 positions of imidazole, respectively. These calculations support the idea that the proton at C5 of imidazole is more acidic than H_2O but less acidic than OH radical. As discussed earlier, the observed photoelectron spectrum of 5-imidazolide had very low intensity. The majority of HO^- ions abstract protons at the N1 position of imidazole, which is much more exothermic than deprotonation at the C5 position (see Figure 4). The DFT calculations show that it is energetically possible for HO^- to deprotonate imidazole at the C2 position; however, there is a very small driving force for this reaction to take place, which probably explains the absence of photoelectron signals from 2-imidazolide (see Figure 3).

It is very difficult to accurately determine the acidity of protons in the presence of more acidic protons in the same molecule. The photoelectron spectrum measurements serve as acidity bracketing experiments for this system. From the gas phase acidities of H_2O and OH radical, $\Delta_{acid}G_{298} = 380 \pm 4$ kcal mol^{-1} is evaluated for the 5-position of imidazole. With the thermochemical properties calculated at the DFT level of theory, D_0(C5−H) $= 119 \pm 4$ kcal mol^{-1} is derived from the thermochemical cycle (eq 7).

Previously, we measured the photoelectron spectrum of pyrrolide.[8] The same ion precursor, HO^-, was used to deprotonate pyrrole, but only the photoelectron spectrum of nitrogen-deprotonated pyrrolide was observed. The DFT calculations give $\Delta_{acid}G_{298} = 387.8$ and 397.6 kcal mol^{-1} at the C2 and C3 positions of pyrrole, respectively. Thus, it is most probable that the protons at the C2 and C3 positions are less acidic than H_2O and that deprotonation does not take place at carbon sites of pyrrole when HO^- is used.

As the DFT calculations suggest in pyrrole, an adjacent N−H group makes a C−H more acidic. However, the acidity of pyrrole at the C2 (or equivalently C5) position is lower than that of imidazole at the C5 position. This comparison indicates that the addition of one more N atom in the five-membered ring results in a significant increase of the acidity. Reactions 11 and 12 show hypothetical proton transfer between pyrrole and imidazole:

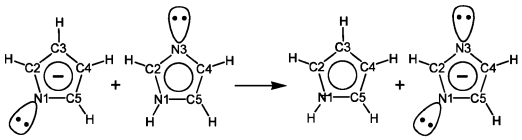

$$\Delta_{rxn}G_{298} = -9.3 \pm 0.6 \text{ kcal mol}^{-1} \quad (11)$$

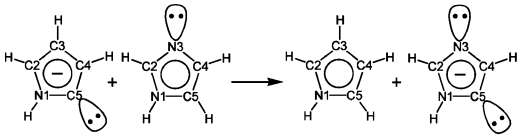

$$\Delta_{rxn}G_{298} = -7.6 \text{ kcal mol}^{-1} \quad (12)$$

Reaction 11 is proton transfer from imidazole to pyrrolide, yielding imidazolide and pyrrole. From the experimental gas phase acidities,[8] the free energy change is $\Delta_{rxn}G_{298} = -9.3 \pm 0.6$ kcal mol^{-1} for this reaction. Taft and co-workers explained the thermodynamics of this reaction with respect to aza-substitution effects.[72,73] They assigned 8.5 kcal mol^{-1} to the stabilization energy of the imidazolide anion due to β-aza substituent. Qualitatively, the same argument applies to the deprotonation at the C5 position of imidazole. Reaction 12 is proton transfer from imidazole to 2-pyrrolide (illustrated as 5-pyrrolide) with 5-imidazolide and pyrrole as products. In the product anion, 5-imidazolide, the lone-pair electron lobe at the C5 position is accompanied by the N lone-pair electron lobe at the β position, analogous to the situation in imidazolide. This β-aza substituent can stabilize 5-imidazolide relative to 2-pyrrolide where there is no aza substituent present. The DFT calculations predict $\Delta_{rxn}G_{298} = -7.6$ kcal mol^{-1} for reaction 12, which may represent the aza substitution effects. Carbon acidities of azines have been discussed in the same way.[100]

The acidity of imidazole at the C2 position is less than that at the C5 position, because deprotonation at C2 produces a repulsive interaction between the lone-pair electron lobes at C2 and N3.[72] This situation contrasts with an imidazole isomer, imidazol-2-ylidene, where the C2 lone-pair electron lobe is flanked by two N−H groups.[101,102] The inductive effects of the N−H groups, together with the mesomeric effects of the π-system, stabilize the singlet carbene.[103]

Conclusion

The photoelectron spectrum of imidazolide, produced by HO^- deprotonation of imidazole in helium buffer gas, has been measured, and the EA of imidazolyl is determined to be 2.613 ± 0.006 eV. Franck−Condon simulation based on the B3LYP/6-311++G(d,p) calculations for the electronic ground states of the anion and neutral reproduces the observed spectrum reasonably well. Two vibrational frequencies of 955 ± 15 and 1365 ± 20 cm^{-1} are active in the spectrum and identified to be totally symmetric modes with C−C stretching and N−C stretching motion, respectively, of $\tilde{X}\ ^2B_1$ imidazolyl. The latter mode, however, mixes with an overtone of an in-plane asymmetric stretching mode through Fermi resonance. Proton transfer rate coefficients for the imidazolide reaction with $(CH_3)_3CSH$ and its reverse reaction have been measured in a FA-SIFT. From these reaction rate coefficients, the gas phase acidity of imidazole is determined to be $\Delta_{acid}G_{298} = 342.6 \pm 0.4$ kcal mol^{-1}, in good agreement with a reported value but with increased precision. With the EA of imidazolyl and the gas phase

acidity of imidazole, the N−H BDE of imidazole is derived using a thermochemical cycle; $D_0(C_3H_3N_2-H) = 95.1 \pm 0.5$ kcal mol^{-1}.

It was found that imidazole is also deprotonated at a carbon site in the reaction with HO^- in the photoelectron spectroscopic measurements. Franck−Condon simulation of the photoelectron spectrum reveals that the deprotonation takes place at the C5 position of imidazole. The EA of 5-imidazolyl is determined to be 1.992 ± 0.010 eV. This spectrum was not observed when O^- was used as a reactant, suggesting that the acidity of the proton at the C5 position of imidazole is bracketed by those of H_2O and OH radical. Thus, the acidity of imidazole at the C5 position is evaluated to be $\Delta_{acid}G_{298} = 380 \pm 4$ kcal mol^{-1}. The acidity is corrected for thermal effects, and combined with the EA of 5-imidazolyl in a thermochemical cycle, the C5−H BDE of imidazole is derived to be $D_0(C5-H) = 119 \pm 4$ kcal mol^{-1}. The relatively large error bar of the C5−H BDE of imidazole arises from the uncertainty of the acidity in the thermochemical cycle. Currently, we are conducting the gas phase acidity measurements of 1-methylimidazole so that we can more accurately determine the carbon acidity of imidazole and, consequently, the C−H BDE.[104]

Acknowledgment. This work was supported by the Air Force Office of Scientific Research and by the National Science Foundation (CHE-0349937, CHE-0512188, and PHY0096822).

References and Notes

(1) Butler, R. N.; Fox, A.; Collier, S.; Burke, L. A. *J. Chem. Soc., Perkin Trans. 2* **1998**, 2243.
(2) Nguyen, M. T.; Ha, T. K. *Chem. Phys. Lett.* **2001**, *335*, 311.
(3) Gagliardi, L.; Orlandi, G.; Evangelisti, S.; Roos, B. O. *J. Chem. Phys.* **2001**, *114*, 10733.
(4) Vij, A.; Pavlovich, J. G.; Wilson, W. W.; Vij, V.; Christe, K. O. *Angew. Chem., Int. Ed.* **2002**, *41*, 3051.
(5) Benin, V.; Kaszynski, P.; Radziszewski, J. G. *J. Org. Chem.* **2002**, *67*, 1354.
(6) Hammerl, A.; Klapotke, T. M. *Inorg. Chem.* **2002**, *41*, 906.
(7) Butler, R. N.; Stephens, J. C.; Burke, L. A. *Chem. Commun.* **2003**, 1016.
(8) Gianola, A. J.; Ichino, T.; Hoenigman, R. L.; Kato, S.; Bierbaum, V. M.; Lineberger, W. C. *J. Phys. Chem. A* **2004**, *108*, 10326.
(9) Gianola, A. J.; Ichino, T.; Hoenigman, R. L.; Kato, S.; Bierbaum, V. M.; Lineberger, W. C. To be published.
(10) Gianola, A. J.; Ichino, T.; Lineberger, W. C.; Stanton, J. F. To be published.
(11) Tommos, C.; Babcock, G. T. *Acc. Chem. Res.* **1998**, *31*, 18.
(12) Pujols-Ayala, I.; Barry, B. A. *Biochim. Biophys. Acta* **2004**, *1655*, 205.
(13) Proshlyakov, D. A.; Pressler, M. A.; DeMaso, C.; Leykam, J. F.; DeWitt, D. L.; Babcock, G. T. *Science* **2000**, *290*, 1588.
(14) Siegbahn, P. E. M.; Blomberg, M. R. A. *Biochim. Biophys. Acta* **2004**, *1655*, 45.
(15) Stubbe, J.; Nocera, D. G.; Yee, C. S.; Chang, M. C. Y. *Chem. Rev.* **2003**, *103*, 2167.
(16) Sealy, R. C.; Harman, L.; West, P. R.; Mason, R. P. *J. Am. Chem. Soc.* **1985**, *107*, 3401.
(17) Hoganson, C. W.; Babcock, G. T. *Biochemistry* **1992**, *31*, 11874.
(18) Spanget-Larsen, J.; Gil, M.; Gorski, A.; Blake, D. M.; Waluk, J.; Radziszewski, J. G. *J. Am. Chem. Soc.* **2001**, *123*, 11253.
(19) Beck, S. M.; Brus, L. E. *J. Chem. Phys.* **1982**, *76*, 4700.
(20) Tripathi, G. N. R.; Schuler, R. H. *J. Chem. Phys.* **1984**, *81*, 113.
(21) Johnson, C. R.; Ludwig, M.; Asher, S. A. *J. Am. Chem. Soc.* **1986**, *108*, 905.
(22) Mukherjee, A.; McGlashen, M. L.; Spiro, T. G. *J. Phys. Chem.* **1995**, *99*, 4912.
(23) Gunion, R. F.; Gilles, M. K.; Polak, M. L.; Lineberger, W. C. *Int. J. Mass Spectrom. Ion Processes* **1992**, *117*, 601.
(24) Navaratnam, S.; Parsons, B. J. *J. Chem. Soc., Faraday Trans.* **1998**, *94*, 2577.
(25) Iwata, S.; Ostermeier, C.; Ludwig, B.; Michel, H. *Nature* **1995**, *376*, 660.
(26) Tsukihara, T.; Aoyama, H.; Yamashita, E.; Tomizaki, T.; Yamaguchi, H.; ShinzawaItoh, K.; Nakashima, R.; Yaono, R.; Yoshikawa, S. *Science* **1996**, *272*, 1136.
(27) Ostermeier, C.; Harrenga, A.; Ermler, U.; Michel, H. *Proc. Natl. Acad. Sci. U.S.A.* **1997**, *94*, 10547.
(28) Yoshikawa, S.; Shinzawa-Itoh, K.; Nakashima, R.; Yaono, R.; Yamashita, E.; Inoue, N.; Yao, M.; Fei, M. J.; Libeu, C. P.; Mizushima, T.; Yamaguchi, H.; Tomizaki, T.; Tsukihara, T. *Science* **1998**, *280*, 1723.
(29) Iwata, S. *J. Biochem.* **1998**, *123*, 369.
(30) Aki, M.; Ogura, T.; Naruta, Y.; Le, T. H.; Sato, T.; Kitagawa, T. *J. Phys. Chem. A* **2002**, *106*, 3436.
(31) Cappuccio, J. A.; Ayala, I.; Elliott, G. I.; Szundi, I.; Lewis, J.; Konopelski, J. P.; Barry, B. A.; Einarsdottir, O. *J. Am. Chem. Soc.* **2002**, *124*, 1750.
(32) Einarsdottir, O.; Szundi, I. *Biochim. Biophys. Acta* **2004**, *1655*, 263.
(33) Rosen, D. R.; Siddique, T.; Patterson, D.; Figlewicz, D. A.; Sapp, P.; Hentati, A.; Donaldson, D.; Goto, J.; Oregan, J. P.; Deng, H. X.; Rahmani, Z.; Krizus, A.; McKennayasek, D.; Cayabyab, A.; Gaston, S. M.; Berger, R.; Tanzi, R. E.; Halperin, J. J.; Herzfeldt, B.; Vandenbergh, R.; Hung, W. Y.; Bird, T.; Deng, G.; Mulder, D. W.; Smyth, C.; Laing, N. G.; Soriano, E.; Pericakvance, M. A.; Haines, J.; Rouleau, G. A.; Gusella, J. S.; Horvitz, H. R.; Brown, R. H. *Nature* **1993**, *362*, 59.
(34) Cleveland, D. W.; Rothstein, J. D. *Nat. Rev. Neurosci.* **2001**, *2*, 806.
(35) Bruijn, L. I.; Houseweart, M. K.; Kato, S.; Anderson, K. L.; Anderson, S. D.; Ohama, E.; Reaume, A. G.; Scott, R. W.; Cleveland, D. W. *Science* **1998**, *281*, 1851.
(36) Johnston, J. A.; Dalton, M. J.; Gurney, M. E.; Kopito, R. R. *Proc. Natl. Acad. Sci. U.S.A.* **2000**, *97*, 12571.
(37) Valentine, J. S. *Free Radical Biol. Med.* **2002**, *33*, 1314.
(38) Zhang, H.; Andrekopoulos, C.; Joseph, J.; Crow, J.; Kalyanaraman, B. *Free Radical Biol. Med.* **2004**, *36*, 1355.
(39) Rakhit, R.; Cunningham, P.; Furtos-Matei, A.; Dahan, S.; Qi, X. F.; Crow, J. P.; Cashman, N. R.; Kondejewski, L. H.; Chakrabartty, A. *J. Biol. Chem.* **2002**, *277*, 47551.
(40) Rakhit, R.; Crow, J. P.; Lepock, J. R.; Kondejewski, L. H.; Cashman, N. R.; Chakrabartty, A. *J. Biol. Chem.* **2004**, *279*, 15499.
(41) Gunther, M. R.; Peters, J. A.; Sivaneri, M. K. *J. Biol. Chem.* **2002**, *277*, 9160.
(42) Alvarez, B.; Demicheli, V.; Duran, R.; Trujillo, M.; Cervenansky, C.; Freeman, B. A.; Radi, R. *Free Radical Biol. Med.* **2004**, *37*, 813.
(43) Samuni, A.; Neta, P. *J. Phys. Chem.* **1973**, *77*, 1629.
(44) The photoelectron spectrum of imidazole has been reported (Cradock, S.; et al. *Tetrahedron* **1973**, *29*, 2173). Vibrational features of imidazole radical cation have been observed in the spectrum, but they have not been analyzed.
(45) Ervin, K. M.; Lineberger, W. C. Photoelectron spectroscopy of negative ions. In *Advances in Gas Phase Ion Chemistry*; Adams, N. G., Babcock, L. M., Eds.; JAI Press: Greenwich, 1992; Vol. 1, p 121.
(46) Leopold, D. G.; Murray, K. K.; Stevens-Miller, A. E.; Lineberger, W. C. *J. Chem. Phys.* **1985**, *83*, 4849.
(47) Ervin, K. M.; Ho, J.; Lineberger, W. C. *J. Chem. Phys.* **1989**, *91*, 5974.
(48) Andersen, T.; Haugen, H. K.; Hotop, H. *J. Phys. Chem. Ref. Data* **1999**, *28*, 1511.
(49) Rienstra-Kiracofe, J. C.; Tschumper, G. S.; Schaefer, H. F.; Nandi, S.; Ellison, G. B. *Chem. Rev.* **2002**, *102*, 231.
(50) Cooper, J.; Zare, R. N. *J. Chem. Phys.* **1968**, *48*, 942.
(51) Van Doren, J. M.; Barlow, S. E.; DePuy, C. H.; Bierbaum, V. M. *Int. J. Mass Spectrom. Ion Processes* **1987**, *81*, 85.
(52) Bierbaum, V. M. Flow tubes. In *Encyclopedia of Mass Spectrometry*; Gross, M. L., Caprioli, R., Eds.; Elsevier: Amsterdam, 2003; Vol. 1, *Theory and Ion Chemistry*, p 276.
(53) Bartmess, J. E.; Scott, J. A.; McIver, R. T., Jr. *J. Am. Chem. Soc.* **1979**, *101*, 6046.
(54) Shiell, R. C.; Hu, X. K.; Hu, Q. J.; Hepburn, J. W. *J. Phys. Chem. A* **2000**, *104*, 4339.
(55) Ervin, K. M.; DeTuro, V. F. *J. Phys. Chem. A* **2002**, *106*, 9947.
(56) Kato, S. Unpublished data.
(57) Su, T.; Chesnavich, W. J. *J. Chem. Phys.* **1982**, *76*, 5183.
(58) Miller, K. J.; Savchik, J. A. *J. Am. Chem. Soc.* **1979**, *101*, 7206.
(59) *CRC Handbook of Chemistry and Physics*, 75 ed.; Lide, D. R., Ed.; CRC Press: Boca Raton, FL, 1994.
(60) Becke, A. D. *J. Chem. Phys.* **1993**, *98*, 5648.
(61) Lee, C. T.; Yang, W. T.; Parr, R. G. *Phys. Rev. B* **1988**, *37*, 785.
(62) Krishnan, R.; Binkley, J. S.; Seeger, R.; Pople, J. A. *J. Chem. Phys.* **1980**, *72*, 650.
(63) Frisch, M. J.; Trucks, G. W.; Schlegel, H. B.; Scuseria, G. E.; Robb, M. A.; Cheeseman, J. R.; Montgomery, J. A., Jr.; Vreven, T.; Kudin, K. N.; Burant, J. C.; Millam, J. M.; Iyengar, S. S.; Tomasi, J.; Barone, V.; Mennucci, B.; Cossi, M.; Scalmani, G.; Rega, N.; Petersson, G. A.; Nakatsuji, H.; Hada, M.; Ehara, M.; Toyota, K.; Fukuda, R.; Hasegama, J.; Ishida, M.; Nakajima, T.; Honda, Y.; Kitao, O.; Nakai, H.; Klene, M.; Li, X.; Knox, J. E.; Hratchian, H. P.; Cross, J. B.; Adamo, C.; Jaramillo, J.; Gomperts, R.; Stratmann, R. E.; Yazyev, O.; Austin, A. J.; Cammi, R.; Pomelli, C.; Ochterski, J. W.; Ayala, P. Y.; Morokuma, K.; Voth, G. A.;

Salvador, P.; Dannenberg, J. J.; Zakrzewski, V. G.; Dapprich, S.; Daniels, A. D.; Strain, M. C.; Farkas, O.; Malick, D. K.; Rabuck, A. D.; Raghavachari, K.; Foresman, J. B.; Ortiz, J. V.; Cui, Q.; Baboul, A. G.; Clifford, S.; Cioslowski, J.; Stefanov, B. B.; Liu, G.; Liashenko, A.; Piskorz, P.; Komaromi, I.; Martin, R. L.; Fox, D. J.; Keith, T.; Al-Laham, M. A.; Peng, C. Y.; Nanayakkara, A.; Challacombe, M.; Gill, P. M. W.; Johnson, B.; Chen, W.; Wong, M. W.; Gonzalez, C.; Pople, J. A. *Gaussian 03, Revision B.05*; Gaussian, Inc.: Pittsburgh, PA, 2004.

(64) Ervin, K. M. *PESCAL, Fortran Program*; http://www.chem.unr.edu/~ervin/pes; University of Nevada, Reno: Reno, NV; 2003.

(65) Ervin, K. M.; Ramond, T. M.; Davico, G. E.; Schwartz, R. L.; Casey, S. M.; Lineberger, W. C. *J. Phys. Chem. A* **2001**, *105*, 10822.

(66) Herzberg, G. *Molecular Specta and Molecular Structure. Vol. II. Infrared and Raman Spectra of Polyatomic Molecules*; Van Nostrand: New York, 1950.

(67) Miani, A.; Cane, E.; Palmieri, P.; Trombetti, A.; Handy, N. C. *J. Chem. Phys.* **2000**, *112*, 248.

(68) Neugebauer, J.; Hess, B. A. *J. Chem. Phys.* **2003**, *118*, 7215.

(69) Boese, A. D.; Martin, J. M. L. *J. Phys. Chem. A* **2004**, *108*, 3085.

(70) Boese, A. D.; Martin, J. M. L. *J. Chem. Phys.* **2004**, *121*, 3405.

(71) NIST Standard Reference Database Number 69; March 2003 Release.

(72) Taft, R. W.; Anvia, F.; Taagepera, M.; Catalan, J.; Elguero, J. *J. Am. Chem. Soc.* **1986**, *108*, 3237.

(73) Catalan, J.; Claramunt, R. M.; Elguero, J.; Laynez, J.; Menendez, M.; Anvia, F.; Quian, J. H.; Taagepera, M.; Taft, R. W. *J. Am. Chem. Soc.* **1988**, *110*, 4105.

(74) Wenthold, P. G.; Polak, M. L.; Lineberger, W. C. *J. Phys. Chem.* **1996**, *100*, 6920.

(75) Without zero-point energy correction.

(76) Gianola, A. J.; Ichino, T.; Lineberger, W. C. Unpublished data.

(77) Ballhaus, C. J.; Hansen, A. E. *Annu. Rev. Phys. Chem.* **1972**, *23*, 15.

(78) Chen, P. Photoelectron spectroscopy of reactive intermediates. In *Unimolecular and Bimolecular Reaction Dynamics*; Ng, C. Y., Baer, T., Powis, I., Eds.; John Wiley & Sons: New York, 1994.

(79) Eiding, J.; Schneider, R.; Domcke, W.; Koppel, H.; Vonniessen, W. *Chem. Phys. Lett.* **1991**, *177*, 345.

(80) Muller, H.; Koppel, H.; Cederbaum, L. S. *New J. Chem.* **1993**, *17*, 7.

(81) Mayer, M.; Cederbaum, L. S.; Koppel, H. *J. Chem. Phys.* **1994**, *100*, 899.

(82) Mahapatra, S.; Koppel, H.; Cederbaum, L. S. *J. Chem. Phys.* **1999**, *110*, 5691.

(83) Applegate, B. E.; Bezant, A. J.; Miller, T. A. *J. Chem. Phys.* **2001**, *114*, 4869.

(84) Cronin, B.; Nix, M. G. D.; Qadiri, R. H.; Ashfold, M. N. R. *Phys. Chem. Chem. Phys.* **2004**, *6*, 5031.

(85) Uchida, K.; Kawakishi, S. *J. Biol. Chem.* **1994**, *269*, 2405.

(86) Bansal, K. M.; Sellers, R. M. *J. Phys. Chem.* **1975**, *79*, 1775.

(87) In basic aqueous solutions, however, formation of imidazolyl radical has been observed. See ref 43.

(88) Tripathi, G. N. R. *J. Am. Chem. Soc.* **1998**, *120*, 4161.

(89) Cradock, S.; Findlay, R. H.; Palmer, M. H. *Tetrahedron* **1973**, *29*, 2173.

(90) DeMatteo, M. P.; Poole, J. S.; Shi, X. F.; Sachdeva, R.; Hatcher, P. G.; Hadad, C. M.; Platz, M. S. *J. Am. Chem. Soc.* **2005**, *127*, 7094.

(91) Llano, J.; Eriksson, L. A. *J. Phys. Chem. B* **1999**, *103*, 5598.

(92) Bu, Y. X.; Cukier, R. I. *J. Phys. Chem. B* **2004**, *108*, 10089.

(93) Kiefer, J. H.; Zhang, Q.; Kern, R. D.; Yao, J.; Jursic, B. *J. Phys. Chem. A* **1997**, *101*, 7061.

(94) Barckholtz, C.; Barckholtz, T. A.; Hadad, C. M. *J. Am. Chem. Soc.* **1999**, *121*, 491.

(95) Shapley, J. R.; Samkoff, D. E.; Bueno, C.; Churchill, M. R. *Inorg. Chem.* **1982**, *21*, 634.

(96) Jones, W. D.; Dong, L. Z.; Myers, A. W. *Organometallics* **1995**, *14*, 855.

(97) Agarwala, R.; Azam, K. A.; Dilshad, R.; Kabir, S. E.; Miah, R.; Shahiduzzaman, M.; Hardcastle, K. I.; Rosenberg, E.; Hursthouse, M. B.; Malik, K. M. A. *J. Organomet. Chem.* **1995**, *492*, 135.

(98) Musaev, D. G.; Morokuma, K. *J. Am. Chem. Soc.* **1995**, *117*, 799.

(99) Blank, D. A.; North, S. W.; Lee, Y. T. *Chem. Phys.* **1994**, *187*, 35.

(100) Meotner, M.; Kafafi, S. A. *J. Am. Chem. Soc.* **1988**, *110*, 6297.

(101) Arduengo, A. J.; Harlow, R. L.; Kline, M. *J. Am. Chem. Soc.* **1991**, *113*, 361.

(102) Arduengo, A. J.; Dias, H. V. R.; Harlow, R. L.; Kline, M. *J. Am. Chem. Soc.* **1992**, *114*, 5530.

(103) Bourissou, D.; Guerret, O.; Gabbai, F. P.; Bertrand, G. *Chem. Rev.* **2000**, *100*, 39.

(104) Villano, S. M.; Gianola, A. J.; Ichino, T.; Kato, S.; Bierbaum, V. M.; Lineberger, W. C. To be published.